iScience

CellPress
OPEN ACCESS

Article

3D spheroid culture synchronizes heterogeneous MSCs into an immunomodulatory phenotype with enhanced anti-inflammatory effects

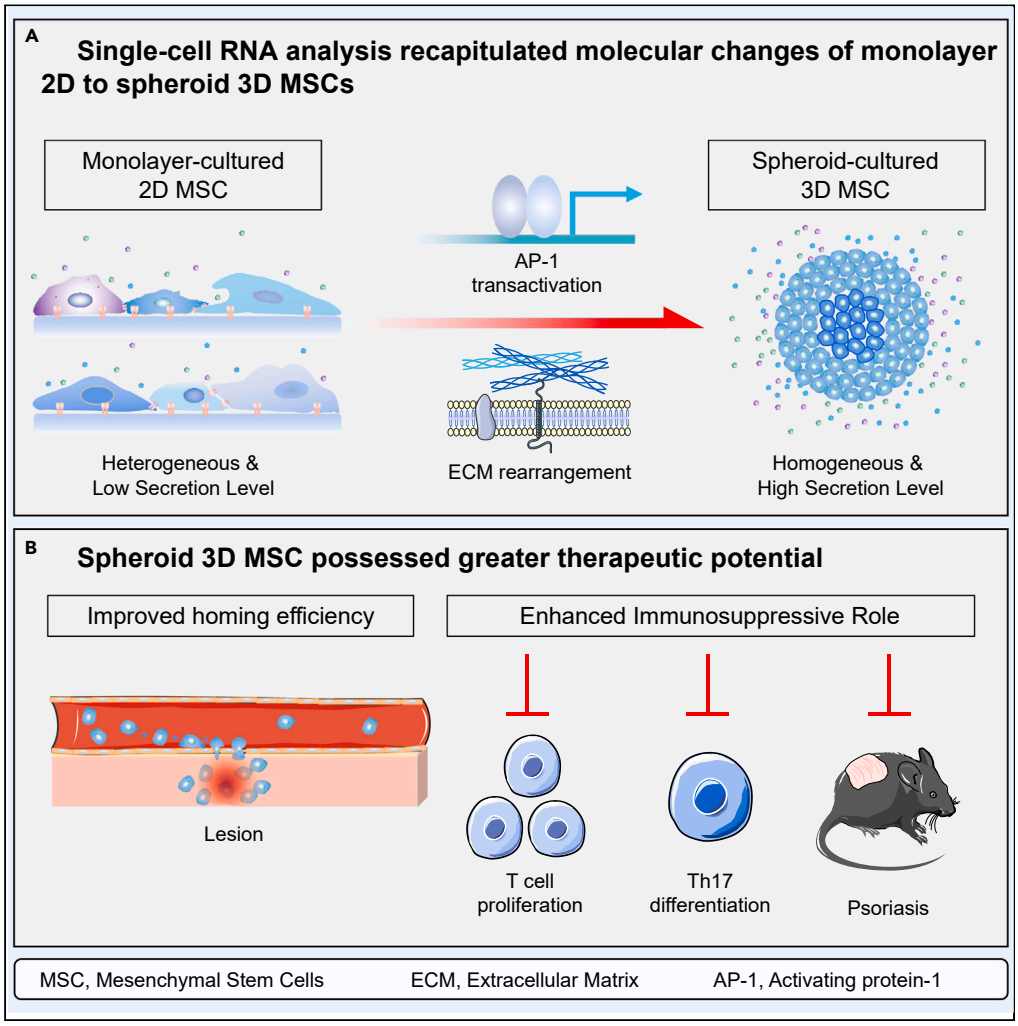

Ruiqing Lu, Ke Zheng, Yongjie Zhou, ..., Guoliang Wang, Yi Zhao, Yaojiong Wu

kara.zheng@sz.tsinghua.edu.cn (K.Z.)
zhaoyimd@tsinghua.edu.cn (Y.Z.)
wu.yaojiong@sz.tsinghua.edu.cn (Y.W.)

Highlights

3D spheroid culture substantially reduces size and heterogenicity of MSCs

3D MSCs exhibit increased homing to inflamed tissues after systemic administration

3D MSCs express higher levels of immunosuppressive factors

3D MSCs show enhanced therapeutic effect on murine psoriasis

Lu et al., iScience 27, 110811
September 20, 2024
https://doi.org/10.1016/j.isci.2024.110811

iScience

CellPress
OPEN ACCESS

Article

3D spheroid culture synchronizes heterogeneous MSCs into an immunomodulatory phenotype with enhanced anti-inflammatory effects

Ruiqing Lu,[1,2,8] Ke Zheng,[1,8,*] Yongjie Zhou,[1,2,8] Weibu Wang,[1] Yanan Zhang,[1] Yu Chen,[1,2] Miaohua Mo,[5] Xiaosong Li,[1] Yankai Dong,[1] Jundong Xie,[1,7] Haiji Zhang,[1,2] Qingyang Yang,[1,6] Guoliang Wang,[7] Yi Zhao,[3,4,*] and Yaojiong Wu[1,6,9,*]

SUMMARY

Mesenchymal stem cells (MSCs) are heterogeneous in morphology and transcriptome, resulting in varying therapeutic outcomes. In this study, we found that 3D spheroid culture of heterogeneous MSCs, which have undergone conventional 2D monolayer culture for 5–6 passages, synchronized the cells into a uniform cell population with dramatically reduced cell size, and considerably increased levels of immunosuppressive genes and growth factors. Single-cell RNA sequencing (scRNA-seq) analysis of the cells revealed that 3D MSCs consisted of 2 major cell subpopulations and both expressed high levels of immunosuppressive factors, compared to 6 subpopulations in 2D MSCs. In addition, 3D MSCs showed a greater suppressive effect on T cells. Moreover, intravenous infusion of a large dose of 3D MSCs prior to imiquimod (IMQ) treatment significantly improved psoriatic lesion. Thus, our results indicate that 3D spheroid culture reprograms heterogeneous MSCs into a uniform immunosuppressive phenotype and promises a novel therapeutic potential for inflammatory diseases.

INTRODUCTION

Since the initial discovery of mesenchymal stem/stromal cells (MSCs) in the bone marrow stroma in rodents in the late 1960s by Friedenstein[1] and further the characterization of the multipotency of cells in humans by Arnold Caplan,[2] the scientific community has been intrigued by the therapeutic potential of these cells. MSCs, known for their multipotent differentiation potential together with their low antigenic properties, quickly became a focal point of regenerative medicine research suitable for allogeneic transplantation.[3–5]

In the current registry of clinical studies hosted on the National Institutes of Health website (clinicaltrials.gov), there are in excess of 1,200 trials concerning MSCs. A majority of these trials spanned across the specialties of traumatology, neurology, cardiology, and immunology, reflecting the versatile nature of MSCs in medical applications.[6–8] Therapeutic interventions utilizing MSCs are primarily predicated upon two distinct mechanisms: firstly, the multipotent differentiation capability of MSCs, which enables them to differentiate into osteoblasts, chondrocytes, and adipocytes, thus facilitating the regeneration and repair of these respective tissues[8,9]; secondly, the paracrine effect exerted by MSCs, which has been considered as the principle mechanism for the therapeutic effects of MSCs in suppressing inflammation and promoting tissue repair, where MSCs secrete a vast array of immunomodulatory cytokines and growth factors, influencing the biological activities and fate of surrounding cells.[7,8]

Despite that MSCs have demonstrated an enormous therapeutic potential for a variety of diseases, there are significant challenges in clinical translation.[5,8] Firstly, the lung entrapment of MSCs after infusion is a significant problem. Intravenous injection is the major administration method for MSCs therapies.[10] However, there are rising concerns over the safety and therapeutic efficiency of systemically administered MSCs. MSCs are significantly enlarged after successive two-dimensional (2D) adherent culture expansion *in vitro*,[11,12] and over 95% of the cells are entrapped in small pulmonary blood vessels after intravenous infusion, which die quickly due to local ischemia caused by vascular obstruction[3,13,14]; this may cause serious clinical outcomes and is attributed to poor therapeutic effects shown in recent clinical trials with

[1]State Key Laboratory of Chemical Oncogenomics, and Institute of Biopharmaceutical and Health Engineering (iBHE), Tsinghua Shenzhen International Graduate School, Tsinghua University, Shenzhen 518055, China
[2]School of Life Sciences, Tsinghua University, Beijing 100084, China
[3]Department of Dermatology, Beijing Tsinghua Changgeng Hospital, School of Clinical Medicine, Tsinghua University, Beijing 102218, China
[4]Photomedicine Laboratory, Institute of Precision Medicine, Tsinghua University, Beijing 102218, China
[5]Department of Biotechnology, Guangdong Medical University, Dongguan 523808, China
[6]Tsinghua-Berkeley Shenzhen Institute, Tsinghua University, Shenzhen 518055, China
[7]Guojian Qingke Biopharmaceutical Co. Ltd, Beijing 100176, China
[8]These authors contributed equally
[9]Lead contact
*Correspondence: kara.zheng@sz.tsinghua.edu.cn (K.Z.), zhaoyimd@tsinghua.edu.cn (Y.Z.), wu.yaojiong@sz.tsinghua.edu.cn (Y.W.)
https://doi.org/10.1016/j.isci.2024.110811

intravenous administration of MSCs.[15,16] Secondly, the heterogenicity of MSCs used for therapies potentially decreases the consistency of effects. Early studies have shown marked variations in morphology and surface receptor expression in MSCs.[17] Recent studies with single-cell RNA sequencing (scRNA-seq) analysis indicate that culture-expanded MSCs are heterogeneous, consisting of osteogenic, chondrogenic, and adipogenic subpopulations, which appear to be progenitors of corresponding tissues, whereas the subpopulations with multipotency and immunoregulation are diminishing with culture expansion,[18,19] potentially affecting their clinical applications.

In this study, we demonstrated that culturing MSCs as three-dimensional (3D) spheroids resulted in cells with markedly reduced size, which barely caused lung entrapment and were abundantly recruited into the skin lesion after intravenous administration. Analysis of bulk and scRNA-seq revealed that the 3D spheroid culture of 2D MSCs for 60 h homogenized the cell population, enriching for an immunosuppressive phenotype with enhanced ability to migrate to inflammation sites and suppress the lesion. This 3D preparation method may allow safer and more effective MSCs treatments by promoting desired therapeutic traits over heterogeneous populations from traditional 2D expansion.

RESULTS

3D spheroid-cultured MSCs exhibit enhanced ability to pass through the lungs

Human placental MSCs, which had been expanded in 2D monolayer culture for 5–6 passages, were cultured in 3D spheroids (scaffold-free) in a cell spinner for 60 h. The cells were examined for the basic features known for MSCs,[20] including the expression of surface markers and trilineage differentiation potency. The results showed that 3D cultured MSCs expressed CD90, CD105, and CD73 in over 95% and CD19, CD34, CD45, human leucocyte antigen DR (HLA-DR), and CD11b in less than 1% of the cells as determined by flow cytometry analysis (Figure 1A) and differentiated into adipocytes, osteoblasts, and chondrocytes upon inductions (Figure 1B), similar to 2D cultured MSCs from the same donor. Consistent with our earlier findings and others,[11,12,21] we noted a marked decrease in MSCs size following spheroid culture (Figures 1C and 1D). When one million of 2D or 3D cultured MSCs, which were pre-labeled with luciferase, were injected into the tail vein, a considerable retention of the cells in the lungs was detected in mice receiving 2D MSCs at 24 h, but minimal amount of cells was found in the lungs in mice receiving 3D MSCs (Figure 1E). The results promised a systemic distribution of 3D cultured MSCs.

3D spheroid culture upregulates the expression of secreted factors

By comparing the transcriptomes of MSCs in 3D spheroid cultures to those in traditional 2D monolayer cultures, we can gain insights into how the 3D environment influences MSCs gene expression and behavior. MSCs in passage 5 of 2D culture or those undergone additional 3D spheroid culture for 60 h were subjected to bulk RNA transcriptome analysis, which included thirty samples from 7 donors (Figure 2A). We used the DESeq2 package to normalize raw counts, and variance stabilizing transforms were applied in order to perform principal-component analysis (PCA). The scatterplot of the first two principal components showed that the two *in vitro* culture methods are the major determinants of the identity of the clusters of samples (Figure 2B). Although the donor identity also played a role in the clustering of samples, the conditions of *in vitro* culture exceeded the natural variations (See Figure S1).

MSCs are known to play a major therapeutic role by secreting factors to regulate immune responses and other cell activities.[4,22] Accordingly, we analyzed the bulk RNA transcriptome datasets based on previous research in terms of gene expression levels and paracrine factors,[23–26] particularly immunosuppressive factors and growth factors (Figure 2Ci/ii).[27,28] The results indicated that several factors known to have immunomodulatory effect such as stanniocalcin-1 (*STC1*), tumor necrosis factor-stimulated protein 6 (*TNFAIP6*, also known as *TSG6*), prostaglandin-endoperoxide synthase 2 (*PTGS2*, the key enzyme in prostaglandin biosynthesis), interleukin 6 (*IL-6*), and transforming growth factor β (*TGF-β*) were substantially upregulated. Meanwhile, many growth factors known to promote tissue regeneration such as vascular endothelial growth factor-α (*VEGFA*), fibroblast growth factor 2 (*FGF2*), leukemia inhibitory factor (*LIF*), hepatocyte growth factor (*HGF*), and glial cell-derived neurotrophic factor (*GDNF*) showed markedly increased expression. The results were confirmed at the levels of mRNA by qPCR (Figure 2D) and protein by ELISA (Figure 2E). Several pathways related to multicellular organism homeostasis were enriched at top levels, suggesting that 3D spheroid culture provides a better *in vivo* microenvironment to modulate the gene expressional sate of MSCs for therapeutic purposes (See Figure S2).

Next, we examined the influence of 3D culture on MSCs aging. MSCs have been known to age *in vitro* upon successive adherent culture expansion, potentially affecting their therapeutic efficacy.[29] The RNA transcriptome analysis revealed that the expression levels of markers negatively associated with passage aging, such as *PTGFRN* and *SERPINF1*,[29] were higher in 3D spheroid-cultured MSCs compared to 2D cultured MSCs (Figure 2Ciii). These results suggest that 3D spheroid culture may have reprogramed MSCs into a more youthful state.

scRNA-seq indicates a predominant immunosuppressive population in 3D spheroid-cultured MSCs

Our earlier results in Figure 1C of this study and previous study[21] showed that MSCs became homogenous in morphology after 3D spheroid culture. We then wanted to know if this was associated with a homogenous gene expression in 3D cultured MSCs and performed scRNA-seq analysis of 2D versus 3D cultured MSCs in passage 5 (EP5), which were derived from the same donor. The data included transcriptomes for 18,075 cells, of which 7,925 were EP5_2D cells and 10,150 were EP5_3D cells. After Seurat integration, unsupervised uniform manifold approximation and projection (UMAP) clustering revealed that 2D and 3D cultured MSCs occurred primarily in discrete clusters with a small fraction of EP5_3D cells clustering together with EP5_2D cells (Figure 3A). With the unbiased UMAP method, we identified 8 clusters in 2D and 3D culture MSCs. The proportion of each cluster in EP5_2D or EP5_3D was plotted, and the name of each cluster was determined based on which sample most of the cells originate from (Figures 3B, 3C, and S3). MSCs cultured in 2D (EP5_2D) retained a heterogeneous nature, whereas

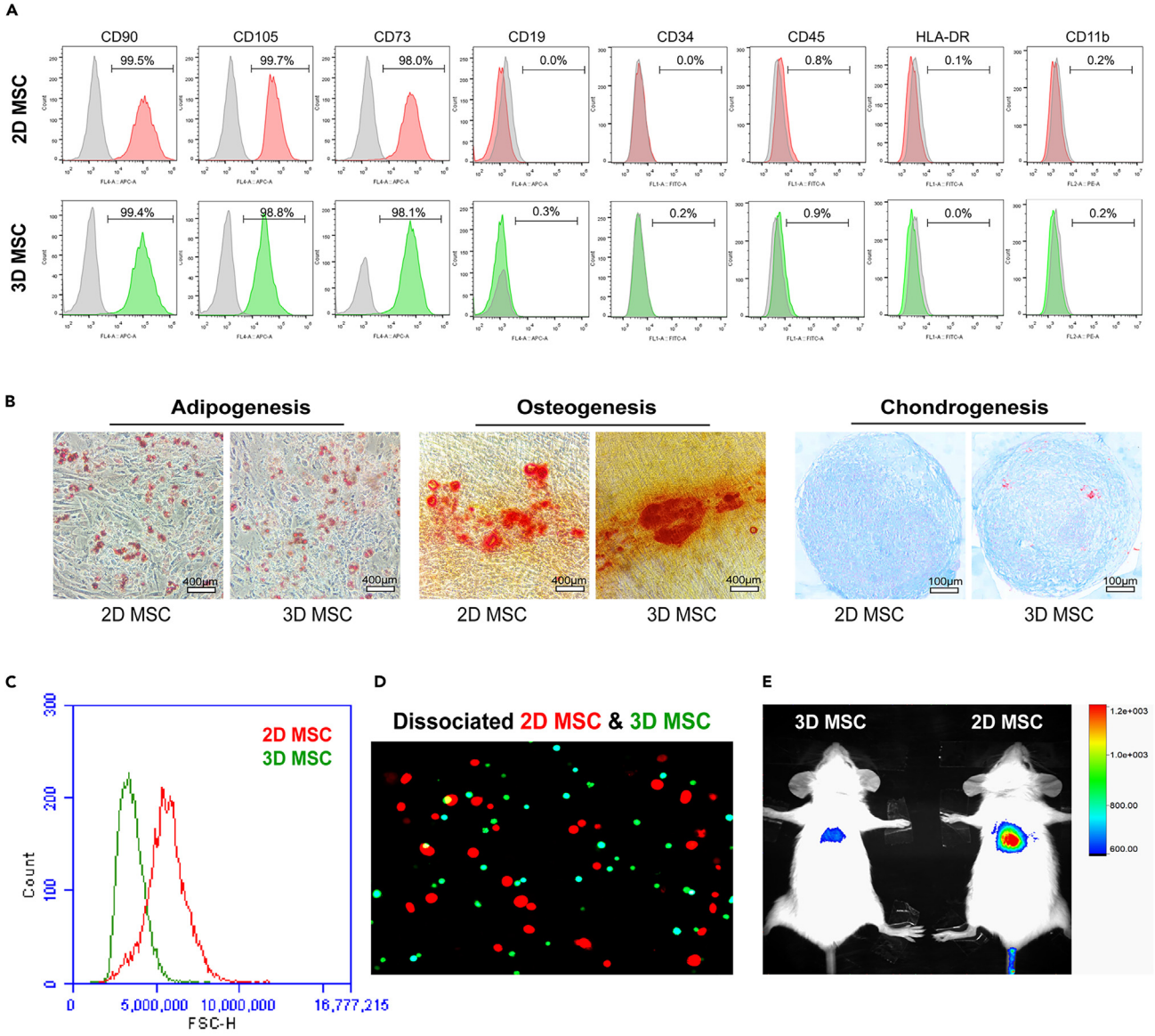

Figure 1. 3D cultured MSCs retain the feature of MSCs but display smaller size and lower lung entrapment

(A) Flow cytometry analysis of 2D and 3D cultured MSCs for surface expression of proteins.

(B) Both 2D and 3D MSCs retained the differentiation potential into adipocytes, osteocytes, and chondrocytes after corresponding induction for 14 days; lipid vesicles in adipocytes were stained with oil red; calcium deposits in osteogenesis were stained with alizarin red; and cells in chondrogenesis were stained with Alcian blue.

(C) Flow cytometry analysis of 2D and 3D MSCs by forward scatter (FSC-H) against counts.

(D) Fluorescent microscope image of dissociated DiI-labeled 2D MSCs and EGFP-tagged 3D MSCs in suspension.

(E) Intravenous injection of 1 × 10^6 2D and 3D MSCs expressing luciferase through mouse tail vein, and luciferase activity was measured after 24 h after injection. Data were obtained from at least three independent experiments or three mice.

those cultured in 3D had only two major clusters. In each cluster, differential expression analysis identified genes that were up- or down-regulated (Figure 3D). Top 5 genes were annotated on the plot. In EP5_3D populations, most of the upregulated genes were associated with immunomodulatory effects, including *STC1*, *TNFAIP6* (*TSG6*), *HGF*, *PTGS2*, and *TGFB1* (Figure 3E). Meanwhile, the two 3D cell clusters also expressed high levels of several growth factors such as *LIF*, *FGF2*, and colony-stimulating factor (*CSF3*), in consistence with our earlier results in transcriptome analysis (Figure 2). Additionally, the two EP5_3D clusters showed higher expression profiles of markers associated with other functional pathways, namely cytokine-paracrine, chemokine-migration, and proliferation-stemness) (Figure 3F). Negative changes of functional pathways are shown in Figure S5.

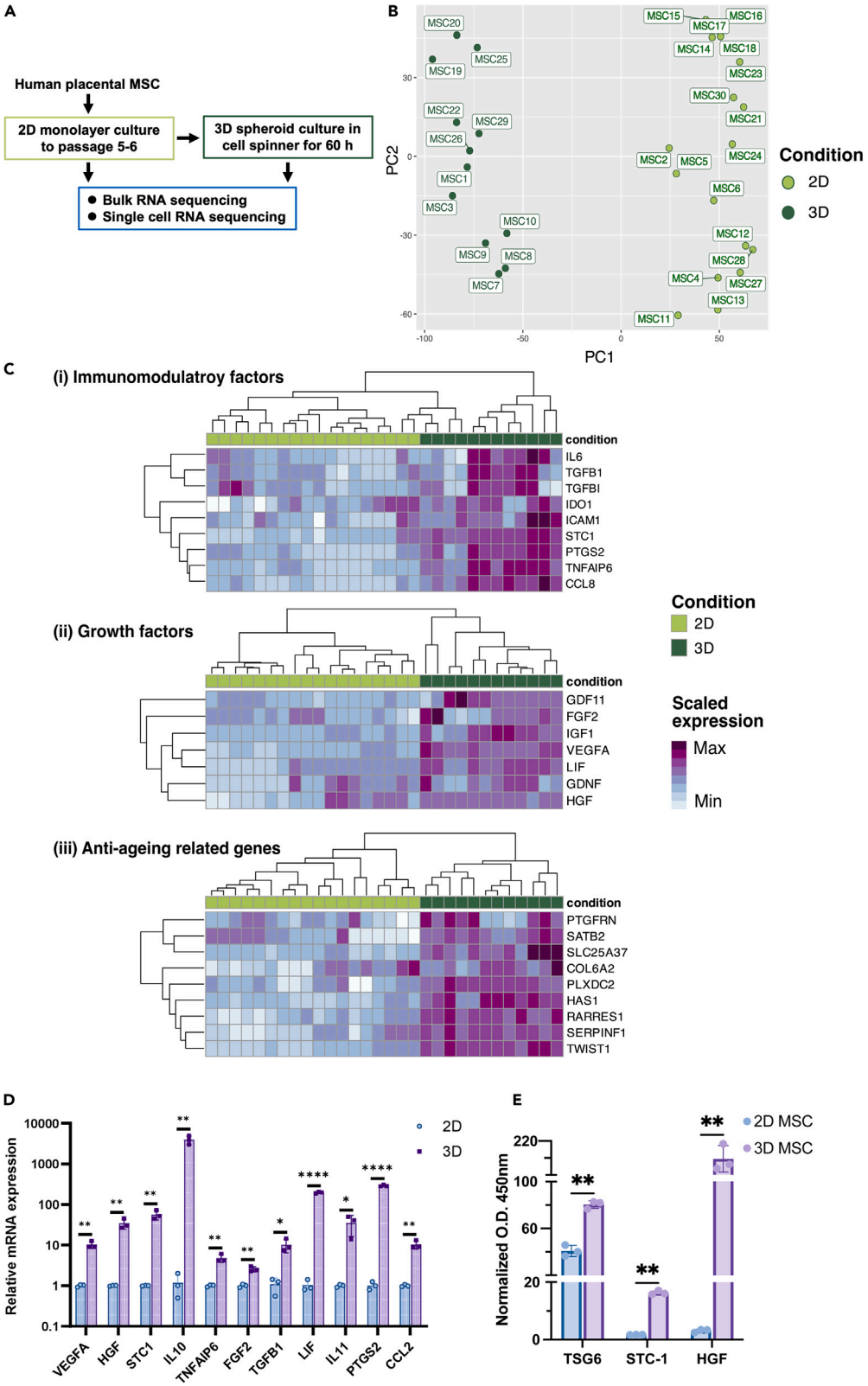
A
Human placental MSC
2D monolayer culture to passage 5-6
3D spheroid culture in cell spinner for 60 h
Bulk RNA sequencing
Single cell RNA sequencing
B
PC1
PC2
Condition
2D
3D
C
(i) Immunomodulatroy factors
condition
IL6
TGFB1
TGFBI
IDO1
ICAM1
STC1
PTGS2
TNFAIP6
CCL8
(ii) Growth factors
GDF11
FGF2
IGF1
VEGFA
LIF
GDNF
HGF
(iii) Anti-ageing related genes
PTGFRN
SATB2
SLC25A37
COL6A2
PLXDC2
HAS1
RARRES1
SERPINF1
TWIST1
Scaled expression
Max
Min
D
Relative mRNA expression
VEGFA
HGF
STC1
IL10
TNFAIP6
FGF2
TGFB1
LIF
IL11
PTGS2
CCL2
E
Normalized O.D. 450nm
2D MSC
3D MSC
TSG6
STC-1
HGF

Figure 2. 3D culture upregulates the expression of immunomodulatory and growth factors of MSCs

(A) Graphical briefing of bulk and single-cell RNA transcriptome experiment and sample submission.

(B) Scatterplot of principal-component analysis (PCA) of the 30 samples from two culture conditions (colored by 2D and 3D MSCs) against the first two PCs analyzed by DESeq2.

(C) Heatmap of immunosuppressive factors (i), growth factors (ii), and anti-ageing markers (iii) expression in 2D and 3D MSCs groups. The relative expression levels were scaled by individual row (gene). Dendrograms show the clustering of individual samples or genes by expression levels. Color schemes annotated by culture conditions (2D/3D) and scaled expression levels.

(D) Quantitative real-time PCR (real-time qPCR) results of relative mRNA expression levels of 2D and 3D MSCs.

(E) ELISA results of protein expression levels of TSG6, STC1, and HGF. Statistical analysis performed as unpaired t test, with p value scheme. Bulk RNA-seq data were collected from 28 samples, including 2D samples (n = 12) and 3D samples (n = 16); qPCR and ELISA data were obtained from three independent experiments. Data are represented as mean ± SD. *: $p < 0.05$; **: $p < 0.01$; ****: $p < 0.0001$.

The results showed 6 clusters in 2D cultured MSCs, which were barely overlapping. Among the clusters, 2D_1 mainly expressed mitotic markers (see Figure S4).[30] Cluster 2D_2 expressed genes in the category of secretion with relatively high expression of paracrine *FGF2*,[31] exosome-related *ANXA1*,[32] and inflammatory response protein *CAV1*.[33] Cluster 2D_3 was considered to be a (passage)-aged stem cell cluster, featured by the expression of cellular senescence genes *CDKN1A*, *LNMA*, and *BTG2*.[34,35] The data also indicated clusters with an early onset of osteogenic cluster 2D_4 (*PTN*, *TCF4*, and *MDK*),[36] adipogenic cluster 2D_5 (*MT2A*, *MT1X*, and *SEC61G*),[37,38] and myogenic cluster 2D_6 (*DDR2*, *PDGFRB*, and *FN1*)[39,40] in 2D cultured MSCs.

Dynverse was used to predict gene expression trajectory within the heterogeneous 2D MSCs population, which was composed of randomly selected 200 cells from each cluster. The slingshot method was predicted to be the most reliable model with a stable trajectory output. A trajectory of four individual branches was obtained from the 2D_2 cluster toward the 2D_3, 2D_4, 2D_5, and 2D_6 clusters (Figure 3H). According to this analysis, 2D_2 was a relatively multipotent cluster within the population that might be capable of differentiating into other clusters. There was a high degree of overlap in gene expression profiles between 2D_3 and 2D_2, since senescence did not show a significant difference in gene expression profiles compared to commitment to differentiation lineages (Figure 3i-first block). While the branching of the slingshot trajectory was distinct, pseudotime analysis indicated a relatively close relationship between the root 2D_2 cluster and individual branches (see Figure S6), which was consistent with previous annotations of individual clusters (Figure 3G) by lineage markers which were expressed at the early stages when cells started commitment to differentiation.

3D MSCs are progressively reprogrammed toward a secretory immunosuppressive phenotype through ECM remodeling and AP-1 complex transactivation

To further understand the biological processes underlying the phenotypic changes observed in 3D MSCs cultured as spheroids, specific clusters were selected from the scRNA-seq analysis for downstream investigation (Figure 4A). Small proportions of cells from each cluster overlapped between 2D and 3D conditions. Gene Ontology analysis of cellular components (GOCC) showed upregulation of genes related to proteinaceous extracellular matrix (ECM), secretory granules, and several transcription factors (e.g., AP-1) in 3D MSCs (Figure 4B).

Based on interpretations from 2D MSCs clusters, cluster 2D_2 represented a multipotent population with differentiation potential toward various lineages within the heterogeneous 2D MSCs population. This cluster also exhibited a highly secretory gene expression profile and was considered the starting point for changes between 2D and 3D conditions. Slingshot trajectory analysis modeled the molecular transitions between 2D and 3D MSCs, showing a linear trajectory from cluster 2D_2 toward cluster 3D_2, passing through an intermediate state in cluster 3D_1 (Figures 4C and 4D).

Detailed gene expression analysis revealed a gradual decrease in collagen components (e.g., *COL6A3*, *COL1A1*, *COL4A1*, *COL4A2*) from clusters 2D_2 to 3D_2, which negatively correlated with increased expression of secretory immunosuppressive factors (e.g., *IL6*, *IL11*, *PTGS2*) (Figure 4E). The importance of the AP-1 transcription factor complex in 3D MSCs was observed. In the trajectory, transient elevation of AP-1 complex members (*FOS*, *JUN*, *JUNB*) connected the decreasing collagen components to the increasing secretory factors, suggesting AP-1 mediates increased expression of immunosuppressive factors upon 3D spheroid culture through ECM modulation. Quantification of mRNA levels corroborated the gradual increase in secretory factors (*VEGFA*, *HGF*, *PTGS2*, *TSG6*) from 2D to 3D spheroid culture conditions (Figure 4F), reinforcing scRNA-seq interpretations of ECM-modulated phenotypic changes. The link between AP-1 and the expression of immunomodulatory genes was further examined by a loss of function assay. Blockade of the function of AP-1 by a specific inhibitor (T5224) markedly decreased the upregulation of *HGF*, *PTGS2*, and *TNFAIP6* (*TSG6* gene) induced by 3D culture as determined by qPCR analysis (Figure 4G). The results suggest that AP-1 functions as a mediator in 3D culture-induced upregulation of immunomodulatory factors.

3D MSCs exert enhanced inhibitory effect on T lymphocyte proliferation and Th17 differentiation

The results of transcriptome analysis of bulk and scRNA-sq analysis suggested that 3D spheroid-cultured MSCs might have an enhanced effect in suppressing inflammation. We examined the effect of 3D MSCs on T cells in culture. The results indicated that 3D MSCs exerted an enhanced effect on suppressing phytohemagglutinin (PHA)-stimulated T cell proliferation (Figures 5A and 5B) and T cell differentiation into Th17 cells (Figures 5C and 5D).

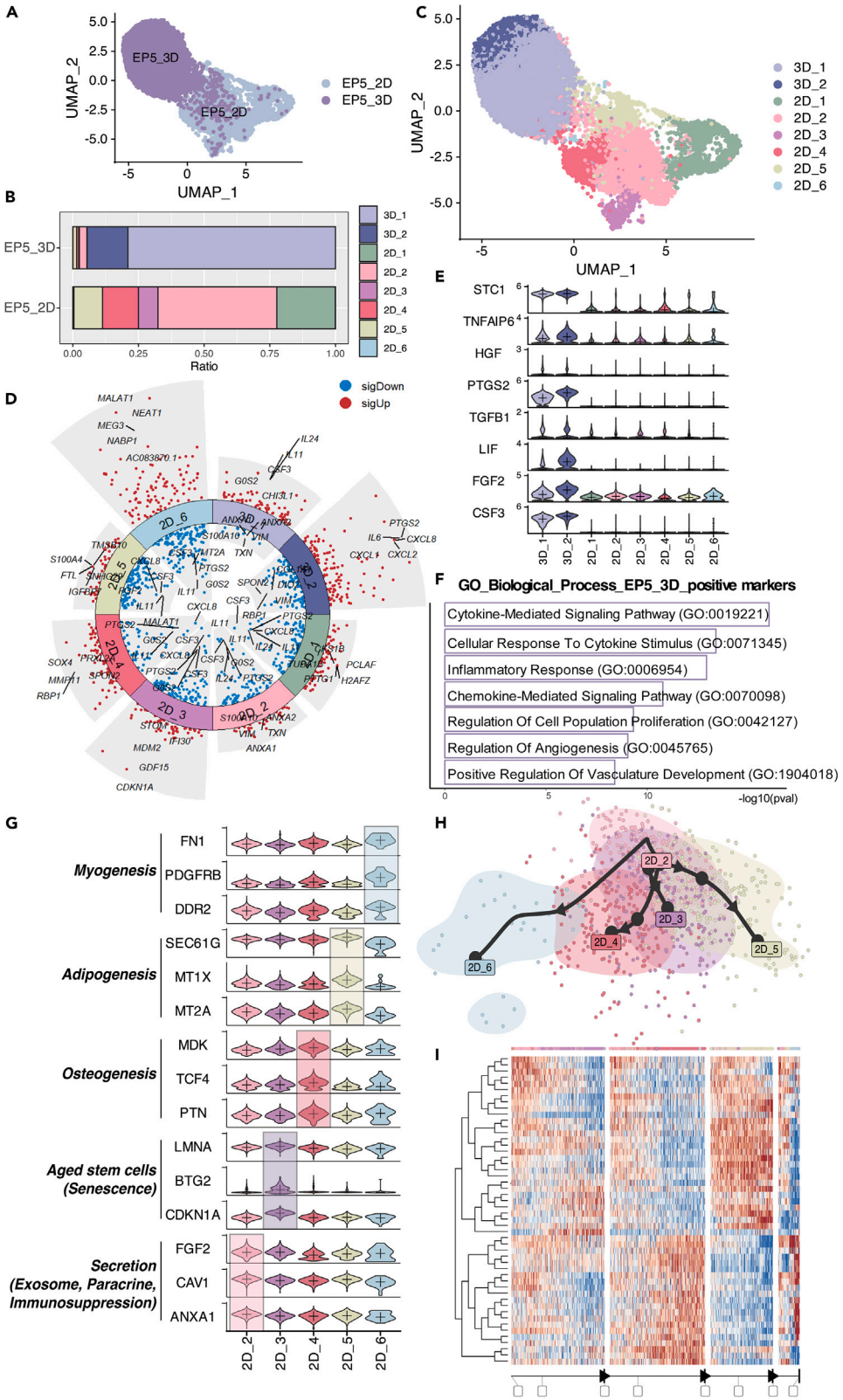
A
EP5_3D
EP5_2D
UMAP_2
UMAP_1
B
EP5_3D
EP5_2D
Ratio
C
3D_1
3D_2
2D_1
2D_2
2D_3
2D_4
2D_5
2D_6
D
sigDown
sigUp
E
STC1
TNFAIP6
HGF
PTGS2
TGFB1
LIF
FGF2
CSF3
F
GO_Biological_Process_EP5_3D_positive markers
Cytokine-Mediated Signaling Pathway (GO:0019221)
Cellular Response To Cytokine Stimulus (GO:0071345)
Inflammatory Response (GO:0006954)
Chemokine-Mediated Signaling Pathway (GO:0070098)
Regulation Of Cell Population Proliferation (GO:0042127)
Regulation Of Angiogenesis (GO:0045765)
Positive Regulation Of Vasculature Development (GO:1904018)
-log10(pval)
G
Myogenesis
FN1
PDGFRB
DDR2
Adipogenesis
SEC61G
MT1X
MT2A
Osteogenesis
MDK
TCF4
PTN
Aged stem cells (Senescence)
LMNA
BTG2
CDKN1A
Secretion (Exosome, Paracrine, Immunosuppression)
FGF2
CAV1
ANXA1
H
I

Figure 3. 3D culture reprograms MSCs into a homogeneous population

(A) UMAP plot of differently cultured MSCs, colored by culture method (EP5_2D n = 7,925, EP5_3D n = 10,150).

(B) Barplot of proportion of Seurat clusters grouped by MSCs culture methods, name given by the dominant identity of culture methods.

(C) UMAP plot of 8 distinct clusters from EP5_2D and EP5_3D groups, with names given by the dominant group for the cluster.

(D) Volcano plot of up- and down-regulated genes in each cluster with minimum expression fraction of 0.25, in which top 5 genes are highlighted by text.

(E) Violin plot of immunosuppression markers of *STC1*, *TNFAIP6*, *HGF*, *PTGS2*, and *TGFB1*.

(F) Enriched pathways in EP5_3D group compare with EP5_2D, analyzed using GO_Biological_Process_2023 database.

(G) Violin plot of three examples of upregulated genes in 2D_2/3/4/5/6 clusters, and manually grouped by established pathways. Cross represents the median value.

(H) Dimension plot of slingshot trajectory of random 200 cells from each EP5_2D clusters (namely 2D_1).

(I) Heatmap of top 50 genes from slingshot trajectory, discrete block as different trajectory branches.

3D cultured MSCs suppress inflammation in psoriasis

To further investigate the effect of 3D cultured MSCs on inflammation in immune diseases, we tested the cells on imiquimod (IMQ)-induced psoriasis model in mice. IMQ is known to induce the development of psoriasis-like lesions in patients when applied to the skin to treat skin diseases.[41] Mice in 4 groups received an intravenous injection of 1 × 10^6 2D cultured MSCs, 1 × 10^6 3D cultured MSCs, 5 × 10^6 3D cultured MSCs (large dose), or an equal volume of PBS (control) 24 h prior to IMQ treatment (Figure 6A). Mice receiving an intravenous injection of 5 × 10^6 3D cultured MSCs did not show abnormal signs, while a significant portion of mice receiving an intravenous injection of 2 × 10^6 2D cultured MSCs died soon after, so the large dose of 2D MSCs group was not examined.

Macroscopic observations indicated that psoriatic lesion developed since one day after topical application of IMQ manifested by the signs of erythema, thickness, and scales on the back skin, and the lesion worsened progressively to day 4 in mice receiving PBS treatment (Figure 6B). We observed improved lesions in mice receiving a large dose of 3D MSCs manifested by less severe erythema, thickening, and scaling with significantly reduced Psoriasis Area and Severity Index (PASI) score (Figure 6C). Lesions in mice receiving 1 × 10^6 2D cultured MSCs or an equal number of 3D MSCs showed a modest improvement (Figure 6C).

Histological analysis of the skin lesion on day 4 following IMQ treatment showed markedly reduced scaling and epidermal thickness along with less keratinocyte proliferation evidenced by fewer Ki67$^+$ mitotic keratinocytes in the basal layer epidermis and the hair follicle in the large-dose 3D MSCs-treated group, compared to the PBS-treated group (Figures 6D–6F). In addition, there was less infiltration of inflammatory cells in the dermis in the large-dose 3D MSCs-treated group (Figure 6D). Notably, we observed the presence of a substantial amount of GFP$^+$ 3D MSCs in the dermis of IMQ-treated skin 5 days after an intravenous infusion of 5 × 10^6 cells (Figure 6F).

DISCUSSION

In this study, we show that culturing MSCs, which have undergone successive expansion in traditional 2D monolayer culture, in 3D spheroids dramatically reduce their size and synchronize them into cells with uniform morphology. In consistence with morphological changes, 3D cultured MSCs show markedly reduced lung entrapment with minimal cell retention following intravenous administration. This allows the cells to enter the systemic blood circulation and migrate into sites of inflammation. So, it is of significance but not surprising to detect a substantial amount of 3D MSCs in the inflamed dermis in the IMQ-treated skin in this study.

The employment of spheroid culture methods in stem cell research has been established over the last three decades, including applications toward tissue regeneration and prolonged *in vitro* stemness. It has been considered that MSCs in spheroids may better mimic the natural *in vivo* microenvironment, where cells more rely on signals mediated by cell-to-cell interactions.[21] The bone marrow MSCs reside in their *in vivo* niches where cell-cell interactions involving N-cadherins are thought to be key to maintaining the stem cell state.[8] When MSCs are cultured *in vitro* as adherent cells, they assemble integrin-based focal adhesions that engage ECM molecules (fibronectin, laminins, and collagens, initially supplied *in vitro* from serum) and form extensive cytoskeletal networks on rigid surface of plastics, glass, and other hard materials.[42] We have shown previously that MSCs cultured in spheroids express higher levels of N-cadherin, whereas 2D monolayer culture of MSCs increases the expression of receptors for cell attachment to ECM molecules such as integrin β1 and α5, leading to increased F-actin assembly.[11,43] Similarly, recent studies have shown that stiffened niches induce skin stem cell aging and differentiation, and blockade of stiffness-mediated Yes-associated protein (YAP) signaling enhanced hair follicle regeneration after wounding.[44,45] These studies suggest that MSCs grown on the rigid polystyrene culture surface are susceptible to spontaneous osteogenic differentiation.[46] This is further supported by our findings in this study and earlier scRNA-seq analysis of MSCs by others, where 2D culture-expanded MSCs contain considerable fractions of cells committed to differentiation of bone and other tissue cell lineages.[18,19] Therefore, increasing evidence indicates that these hard surfaces are not appropriate to retain the multipotency of MSCs.

It has been considered that the therapeutic effects of MSCs on tissue injuries and inflammation largely rely on their secretion of immunomodulatory factors. Previous studies have identified several secreted factors crucial for the suppressive effect of MSCs on inflammatory conditions, such as STC1, TSG6, HGF, IDO1, PGE2, and TGF-β.[7,8] TSG6 has been found to facilitate the transition of macrophages from the pro-inflammatory M1 phenotype to the anti-inflammatory M2 phenotype.[47] Prophylactic injection of human MSCs in mice has been demonstrated to prevent allogeneic corneal transplant rejection in mice, potentially through TSG6-mediated induction of macrophage immune tolerance.[48] Additionally, STC1 inhibits the recruitment of CD14$^+$ monocytes/macrophages, thereby exerting an anti-inflammatory effect.[23] Moreover, HGF suppresses the activation and release of pro-inflammatory cytokines of many types of immune cells, such as dendritic cells, T cells, B cells, and neutrophils and ultimately prevent the activation of nuclear factor (NF)-κB. Thus HGF regulates central inflammatory events

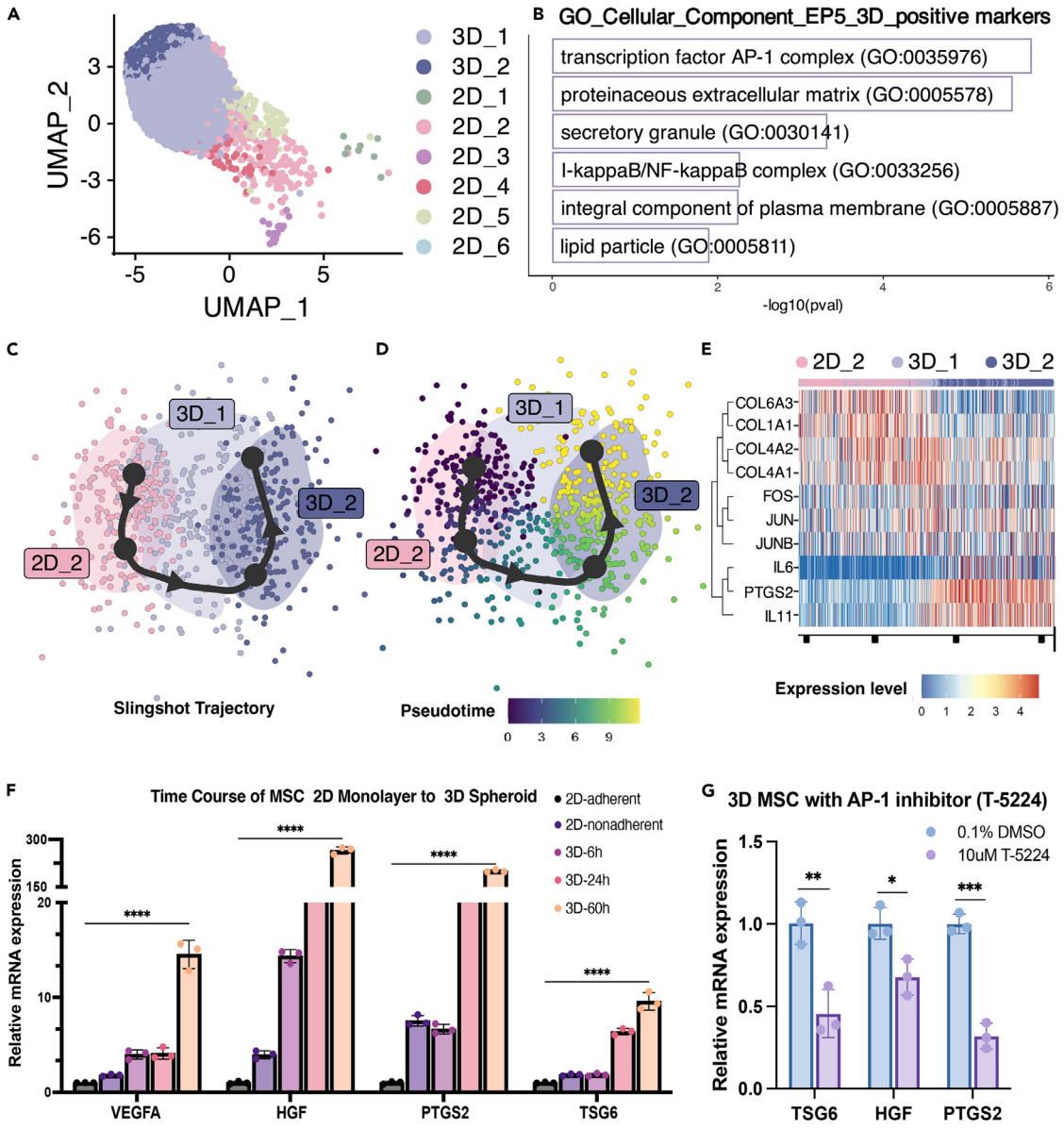

Figure 4. The transition of MSCs toward a secretory immunosuppressive phenotype in 2D to 3D culture

(A) UMAP plot of 8 distinct clusters from EP5_3D groups, subset from the integrated dataset.

(B) Barplot of enriched pathways in EP5_3D group compared with EP5_2D, analyzed using GO_Cellualr_Component_2023 database.

(C and D) Dimension plot of slingshot trajectory of random 200 cells from EP5_3D (2D_2, 3D_1, and 3D_2) clusters, colored by cluster and (D) pseudotime.

(E) Heatmap of collagens (*COL6A3*, *COL1A1*, *COL4A1*, and *COL4A2*), AP-1 complex (*FOS*, *JUN*, and *JUNB*), and immunomodulatory factors (*IL6*, *IL11*, and *PTGS2*).

(F and G) qPCR results of relative mRNA expression levels (Log10 years axis) of MSCs in 2D adherent culture, non-adherent culture, and 3D spheroid culture for different times (6, 24, and 60 h) (F), and MSCs cultured in 3D spheroid in the absence and presence of an AP-1 inhibitor (T5224) for 24 h (G). Results of qPCR were obtained from three independent experiments. Data are represented as mean ± SD. Statistical analyses performed in (F) and (G) are one-way ANOVA and unpaired t test, respectively. *: $p < 0.05$; **: $p < 0.01$; ***: $p < 0.001$; ****: $p < 0.0001$.

that are common to many diseases and organ systems[49] and is shown to be crucial for the effect of MSCs in alleviating autoimmune encephalomyelitis in mice.[26]

In this study, our bulk RNA-seq of MSCs from several donors showed that 3D spheroid culture significantly upregulated the expression levels of immunomodulatory factors such as *STC1*, *TSG6*, *HGF*, *TGF-β*, and *PTGS2*. This is consistent with several previous studies.[25,50,51] Interestingly, scRNA-seq analysis of 3D spheroid-cultured MSCs displayed a dramatically enlarged cell pool to include almost all cells expressing high levels of the immunomodulatory factors. This implies an enhanced immunoregulatory function of 3D cultured MSCs. Indeed, we found

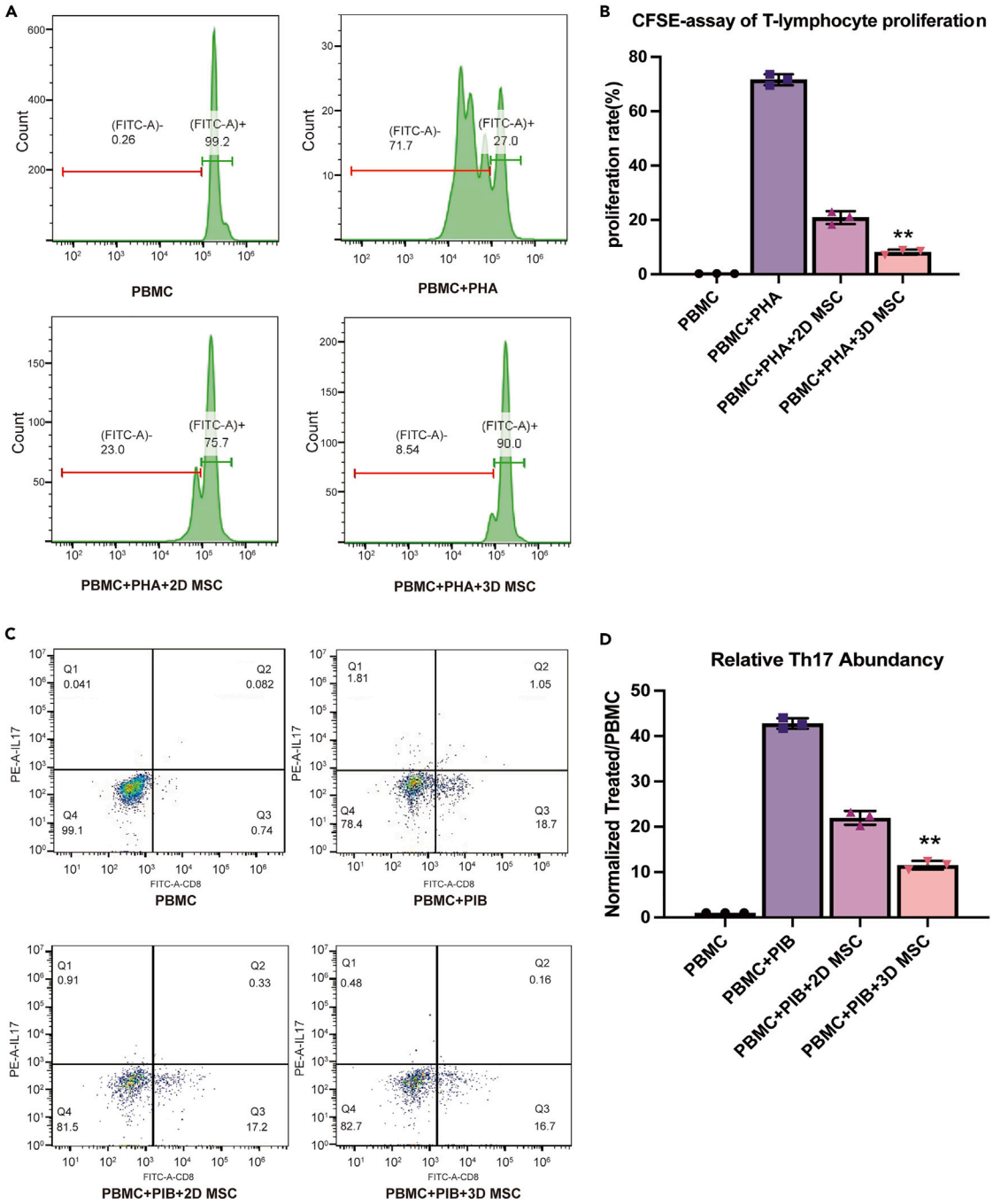

Figure 5. 3D MSCs exert enhanced inhibitory effect on T lymphocyte proliferation and Th17 differentiation

(A and B) Flow cytometry of carboxyfluorescein diacetate succinimidyl ester (CFSE)-assay on PHA-stimulated PBMC T cell proliferation, fluorescein isothiocyanate $(FITC)^{-}$ population marks for the proportion of proliferating cells (A), and the results show a greater inhibitory effect of 3D MSCs on T cell proliferation (B; **, p value = 0.0088, one-way ANOVA).

(C and D) Flow cytometry analysis of PIB (PMA/Ionomycin/BFA) stimulated PBMC differentiation into Th17 subpopulation (Q1 $CD8^{-}IL17^{+}$, C), and the results show a significant decrease in the number of Th17 cells after 3D MSCs treatment (D. **, p value = 0.0011, one-way ANOVA). Data were obtained from three independent experiments. Data are represented as mean ± SD. Phorbol 12-myristate 13-acetate (PMA).

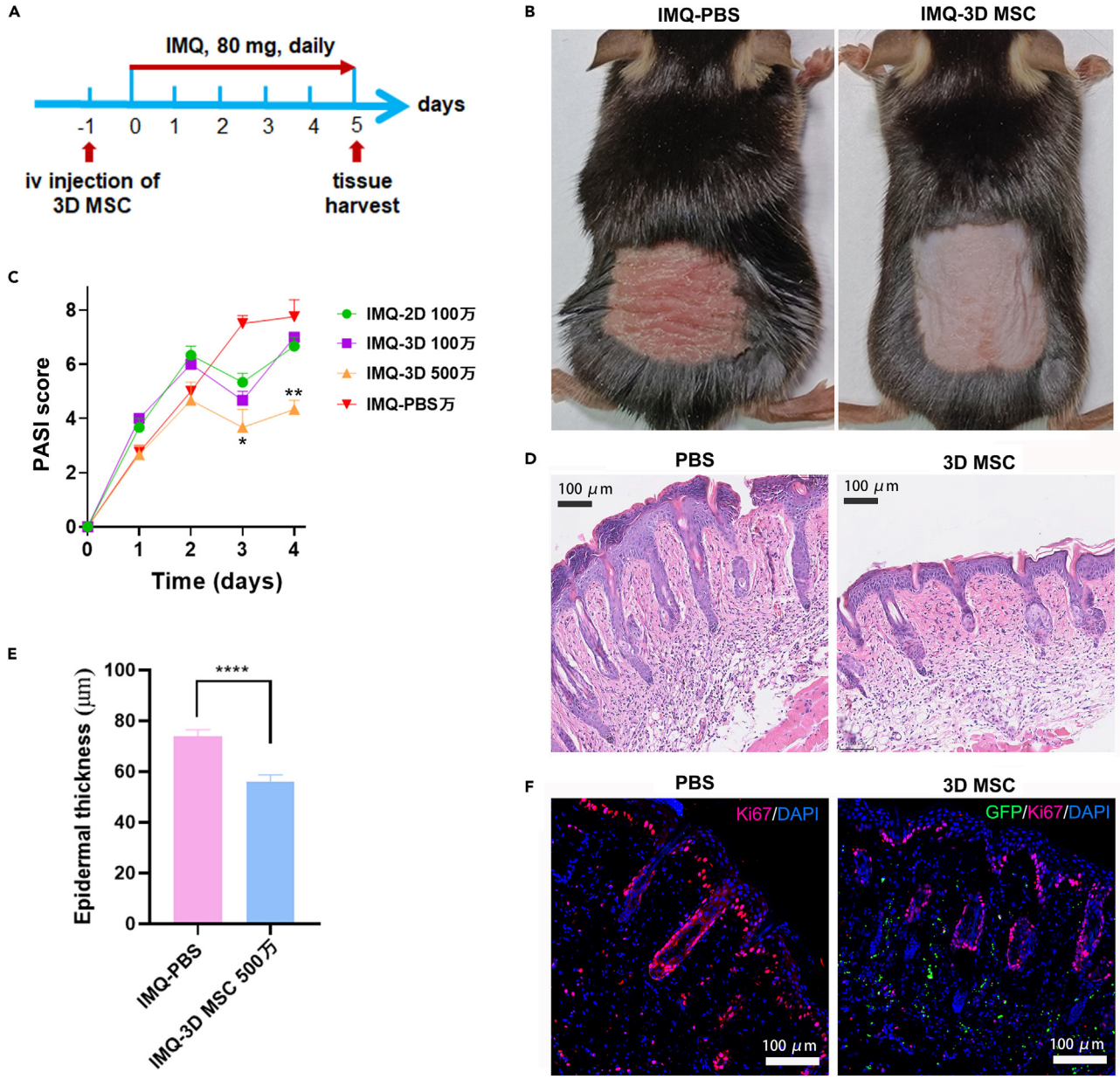

Figure 6. 3D cultured MSCs suppress psoriatic inflammation

(A) Graphical briefing of MSCs treatment in psoriasis disease model, where mice received a tail vein injection of 1 × 10^6 of 2D cultured MSCs, 1 × 10^6 of 3D cultured MSCs, a large dose (5 × 10^6) of 3D cultured MSCs, or an equal volume of PBS (control) 24 h prior to imiquimod (IMQ) treatment, which was topically applied to the back skin 80 mg daily.

(B) Representative images of mice in control group (IMQ-PBS) or large dose of 3D MSCs-treated group (IMQ-3D MSCs) after IMQ treatment for 4 days.

(C) Quantification of Psoriasis Area and Severity Index (PASI) score every day of different experimental groups, p value = 0.0077 (**).

(D) Hematoxylin and Eosin (H&E) staining of skin samples from day 4 IMQ-PBS or IMQ-3D MSCs-treated mice.

(E) Measurement of epidermal thickness on H&E-stained day 4 skin sections, using unpaired t test, p value < 0.0001 (****).

(F) Immunofluorescence of Ki67 and GFP-tagged MSCs of skin samples from day 4 IMQ-PBS or IMQ-3D MSCs-treated mice. Data were collected from at least three independent experiments or three mice. Data are represented as mean ± SD. Statistical analysis performed in (C) and (E) are one-way ANOVA.

that 3D MSCs exhibited a greater inhibitory effect on T lymphocyte proliferation upon stimulation (Figure 5). Notably, when intravenously administered prior to IMQ application, 3D MSCs significantly decreased IMQ-induced psoriatic lesion in mice. Recently it has been shown that MSCs primed by inflammatory cytokines alleviate psoriasis-like inflammation via the TSG6-neutrophil axis.[52] In has been well known that 2D cultured MSCs are barely detected in tissues outside of the lungs after intravenous injection.[15] In this study, however, we found

that 3D MSCs were present abundantly in IMQ-induced skin lesion, where MSCs were likely to secret immunosuppressive factors such as TSG6 to inhibit the inflammation.

Our scRNA-seq analysis indicated a remarkable transition of MSCs toward homogeneity during 3D spheroid culture. We detected 6 subpopulations in 2D monolayer cultured expanded MSCs, which were largely non-overlapping. This is in consistence with several recent studies, where different clusters with distinctive gene expression toward different tissue lineages were found in 2D cultured MSCs derived from different tissues.[18,19] In our previous study, we showed that 3D culture reduced F-actin assembly and enhanced vesicle excretion in MSCs, leading to reduced cell size and increased morphological homogeneity.[12] Here, scRNA-seq demonstrated that 3D spheroid culture generates a homogeneous cell population containing only two major overlapping clusters, with one cluster predominating. Compared to 2D culture, 3D spheroids reprogrammed MSCs toward a secretory phenotype, as evidenced by enhanced expression of growth factors and immunosuppressive factors. We propose this reprogramming process is regulated by changes in collagen ECM composition and activation of the AP-1 transcription factor complex. AP-1 complex's critical role in immune regulation has been well documented.[53] However, whether collagen directly or indirectly regulates AP-1 as upstream effectors remains to be further elucidated.

Taken together, we found that 3D spheroid culture synchronizes heterogeneous MSCs into a homogenous population expressing high levels of immunomodulatory factors. 3D cultured MSCs show enhanced suppression to lymphocyte proliferation and improve inflammatory lesion in psoriatic mouse model. Our results promise a safer and more effective therapeutic potential of 3D spheroid culture MSCs for inflammatory diseases.

Limitations of the study

As mentioned in this study, the scRNA-seq analysis suggests that the transactivation of AP-1 may be responsible for the 2D MSCs to 3D MSCs change, especially the enhanced immunomodulatory function of 3D MSCs. However, further experimental proof is required. In addition, 3D MSCs have a more uniform and smaller cell size and a stronger secretion capacity, and the mechanisms involved still need to be further clarified.

RESOURCE AVAILABILITY

Lead contact

Further information and requests for resources, reagents, and protocols should be directed to and will be fulfilled by the lead contact, Wu Yaojiong (wu.yaojiong@sz.tsinghua.edu.cn).

Materials availability

This study did not generate new unique reagents.

Data and code availability

- scRNA-seq data have been deposited at GEO and are publicly available as of the date of publication. Accession numbers are listed in the key resources table. qPCR data reported in this paper will be shared by the lead contact upon reasonable request.
- All original code has been deposited at Zenodo and is publicly available as of the date of publication. DOIs are listed in the key resources table.
- Any additional information required to reanalyze the data reported in this paper is available from the lead contact upon request.

ACKNOWLEDGMENTS

This work was supported by grants from the National Key R&D Program of China (2023YFA0914300), Shenzhen Science and Technology Innovation Committee (GJHZ20220913143002005), State Key Laboratory of Chemical Oncogenomics fund, Tsinghua Shenzhen International Graduate School Overseas Cooperation Fund (HW2021003), Guangdong Basic and Applied Basic Research Foundation (2022A1515011696), and Dongguan Science and Technology of Social Development Program (20221800905572).

AUTHOR CONTRIBUTIONS

Conceptualization, Y.W. and Y.Zhao; methodology, R.L., K.Z., and Y.Zhou; formal analysis, R.L., K.Z., and Y.Zhou; investigation, R.L., K.Z., Y.Zhou, W.W., Y.Zhang, Y.C., M.M., X.L., Y.D., J.X., H.Z., and Q.Y.; resources, Y.W., Y.Zhao, and G.W.; writing – original draft, K.Z.; writing – review and editing, Y.W. and Y.Zhao; visualization, R.L., K.Z., and Y.Zhou; supervision, Y.W. and Y.Zhao; project administration, Y.W. and Y.Zhao; funding acquisition, Y.W. and Y.Zhao

DECLARATION OF INTERESTS

The authors declare no competing interests.

STAR★METHODS

Detailed methods are provided in the online version of this paper and include the following:

- Transduction of MSCs (GFP/Luciferase)
- Flow cytometry
- Trilineage differentiation
- Bioluminescence imaging
- Bulk RNA sequencing and quantitative real-time PCR (qPCR)
- Single-cell RNA sequencing (scRNA-seq)
- PBMC stimulation and CFSE assay
- Cytokine quantification by ELISA
- Histology

- MSCS ADMINISTRATION TO PSORIASIS MOUSE MODEL
- QUANTIFICATION AND STATISTICAL ANALYSIS

SUPPLEMENTAL INFORMATION

Supplemental information can be found online at https://doi.org/10.1016/j.isci.2024.110811.

Received: June 6, 2024
Revised: July 16, 2024
Accepted: August 21, 2024
Published: August 24, 2024

REFERENCES

1. Friedenstein, A.J., Petrakova, K.V., Kurolesova, A.I., and Frolova, G.P. (1968). Heterotopic of bone marrow. Analysis of precursor cells for osteogenic and hematopoietic tissues. Transplantation *6*, 230–247.
2. Caplan, A.I. (1991). Mesenchymal stem cells. J. Orthop. Res. *9*, 641–650. https://doi.org/10.1002/jor.1100090504.
3. Ankrum, J.A., Ong, J.F., and Karp, J.M. (2014). Mesenchymal stem cells: immune evasive, not immune privileged. Nat. Biotechnol. *32*, 252–260. https://doi.org/10.1038/NBT.2816.
4. Han, Y., Yang, J., Fang, J., Zhou, Y., Candi, E., Wang, J., Hua, D., Shao, C., and Shi, Y. (2022). The secretion profile of mesenchymal stem cells and potential applications in treating human diseases. Signal Transduct. Targeted Ther. *7*, 92. https://doi.org/10.1038/s41392-022-00932-0.
5. Galipeau, J., and Sensébé, L. (2018). Mesenchymal Stromal Cells: Clinical Challenges and Therapeutic Opportunities. Cell Stem Cell *22*, 824–833. https://doi.org/10.1016/J.STEM.2018.05.004.
6. Rodriguez-Fuentes, D.E., Fernandez-Garza, L.E., Samia-Meza, J.A., Barrera-Barrera, S.A., Caplan, A.I., and Barrera-Saldana, H.A. (2021). Mesenchymal Stem Cells Current Clinical Applications: A Systematic Review. Arch. Med. Res. *52*, 93–101. https://doi.org/10.1016/j.arcmed.2020.08.006.
7. Zhou, J., and Shi, Y. (2023). Mesenchymal stem/stromal cells (MSCs): origin, immune regulation, and clinical applications. Cell. Mol. Immunol. *20*, 555–557. https://doi.org/10.1038/s41423-023-01034-9.
8. Pittenger, M.F., Discher, D.E., Péault, B.M., Phinney, D.G., Hare, J.M., and Caplan, A.I. (2019). Mesenchymal stem cell perspective: cell biology to clinical progress. NPJ Regen. Med. *4*, 22. https://doi.org/10.1038/s41536-019-0083-6.
9. Chamberlain, G., Fox, J., Ashton, B., and Middleton, J. (2007). Concise review: mesenchymal stem cells: their phenotype, differentiation capacity, immunological features, and potential for homing. Stem Cell. *25*, 2739–2749.
10. Musial-Wysocka, A., Kot, M., and Majka, M. (2019). The Pros and Cons of Mesenchymal Stem Cell-Based Therapies. Cell Transplant. *28*, 801–812. https://doi.org/10.1177/0963689719837897.
11. Wang, S., Guo, L., Ge, J., Yu, L., Cai, T., Tian, R., Jiang, Y., Zhao, R.C., and Wu, Y. (2015). Excess Integrins Cause Lung Entrapment of Mesenchymal Stem Cells. Stem Cell. *33*, 3315–3326. https://doi.org/10.1002/stem.2087.
12. Mo, M., Zhou, Y., Li, S., and Wu, Y. (2018). Three-Dimensional Culture Reduces Cell Size By Increasing Vesicle Excretion. Stem Cell. *36*, 286–292. https://doi.org/10.1002/stem.2729.
13. Lee, R.H., Pulin, A.A., Seo, M.J., Kota, D.J., Ylostalo, J., Larson, B.L., Semprun-Prieto, L., Delafontaine, P., and Prockop, D.J. (2009). Intravenous hMSCs improve myocardial infarction in mice because cells embolized in lung are activated to secrete the anti-inflammatory protein TSG-6. Cell Stem Cell *5*, 54–63. https://doi.org/10.1016/j.stem.2009.05.003.
14. Toma, C., Wagner, W.R., Bowry, S., Schwartz, A., and Villanueva, F. (2009). Fate Of Culture-Expanded Mesenchymal Stem Cells in The Microvasculature: In Vivo Observations of Cell Kinetics. Circ. Res. *104*, 398–402. https://doi.org/10.1161/circresaha.108.187724.
15. Wu, Z., Zhang, S., Zhou, L., Cai, J., Tan, J., Gao, X., Zeng, Z., and Li, D. (2017). Thromboembolism Induced by Umbilical Cord Mesenchymal Stem Cell Infusion: A Report of Two Cases and Literature Review. Transplant. Proc. *49*, 1656–1658. https://doi.org/10.1016/j.transproceed.2017.03.078.
16. Hess, D.C., Wechsler, L.R., Clark, W.M., Savitz, S.I., Ford, G.A., Chiu, D., Yavagal, D.R., Uchino, K., Liebeskind, D.S., Auchus, A.P., et al. (2017). Safety and efficacy of multipotent adult progenitor cells in acute ischaemic stroke (MASTERS): a randomised, double-blind, placebo-controlled, phase 2 trial. Lancet Neurol. *16*, 360–368. https://doi.org/10.1016/S1474-4422(17)30046-7.
17. Wegmeyer, H., Bröske, A.M., Leddin, M., Kuentzer, K., Nisslbeck, A.K., Hupfeld, J., Wiechmann, K., Kuhlen, J., von Schwerin, C., Stein, C., et al. (2013). Mesenchymal stromal cell characteristics vary depending on their origin. Stem Cell. Dev. *22*, 2606–2618. https://doi.org/10.1089/scd.2013.0016.
18. Xie, Z., Yu, W., Ye, G., Li, J., Zheng, G., Liu, W., Lin, J., Su, Z., Che, Y., Ye, F., et al. (2022). Single-cell RNA sequencing analysis of human bone-marrow-derived mesenchymal stem cells and functional subpopulation identification. Exp. Mol. Med. *54*, 483–492. https://doi.org/10.1038/s12276-022-00749-5.
19. Sun, C., Wang, L., Wang, H., Huang, T., Yao, W., Li, J., and Zhang, X. (2020). Single-cell RNA-seq highlights heterogeneity in human primary Wharton's jelly mesenchymal stem/stromal cells cultured in vitro. Stem Cell Res. Ther. *11*, 149. https://doi.org/10.1186/s13287-020-01660-4.
20. Viswanathan, S., Blanc, K.L., Ciccocioppo, R., Dagher, G., Filiano, A.J., Galipeau, J., Krampera, M., Krieger, L., Lalu, M.M., Nolta, J., et al. (2023). An International Society for Cell and Gene Therapy Mesenchymal Stromal Cells (MSC) Committee perspectives on International Standards Organization/Technical Committee 276 Biobanking Standards for bone marrow-MSCs and umbilical cord tissue–derived MSCs for research purposes. Cytotherapy *25*, 803–807. https://doi.org/10.1016/j.jcyt.2023.04.005.
21. Bartosh, T.J., Ylöstalo, J.H., Mohammadipoor, A., Bazhanov, N., Coble, K., Claypool, K., Lee, R.H., Choi, H., and Prockop, D.J. (2010). Aggregation of human mesenchymal stromal cells (MSCs) into 3D spheroids enhances their antiinflammatory properties. Proc. Natl. Acad. Sci. USA *107*, 13724–13729. https://doi.org/10.1073/pnas.1008117107.
22. Wang, Y., Fang, J., Liu, B., Shao, C., and Shi, Y. (2022). Reciprocal regulation of mesenchymal stem cells and immune responses. Cell Stem Cell *29*, 1515–1530. https://doi.org/10.1016/j.stem.2022.10.001.
23. Mohammadipoor, A., Lee, R.H., Prockop, D.J., and Bartosh, T.J. (2016). Stanniocalcin-1 attenuates ischemic cardiac injury and response of differentiating monocytes/macrophages to inflammatory stimuli. Transl. Res. *177*, 127–142. https://doi.org/10.1016/J.TRSL.2016.06.011.
24. Mittal, M., Tiruppathi, C., Nepal, S., Zhao, Y.Y., Grzych, D., Soni, D., Prockop, D.J., and Malik, A.B. (2016). TNFα-stimulated gene-6 (TSG6) activates macrophage phenotype transition to prevent inflammatory lung injury.

Proc. Natl. Acad. Sci. USA *113*, E8151–E8158. https://doi.org/10.1073/PNAS.1614935113.

25. Bartosh, T.J., Ylöstalo, J.H., Bazhanov, N., Kuhlman, J., and Prockop, D.J. (2013). Dynamic compaction of human mesenchymal stem/precursor cells into spheres self-activates caspase-dependent IL1 signaling to enhance secretion of modulators of inflammation and immunity (PGE2, TSG6, and STC1). Stem Cell. *31*, 2443–2456. https://doi.org/10.1002/STEM.1499.
26. Bai, L., Lennon, D.P., Caplan, A.I., DeChant, A., Hecker, J., Kranso, J., Zaremba, A., and Miller, R.H. (2012). Hepatocyte growth factor mediates mesenchymal stem cell–induced recovery in multiple sclerosis models. Nat. Neurosci. *15*, 862–870. https://doi.org/10.1038/nn.3109.
27. Haghighitalab, A., Matin, M.M., Amin, A., Minaee, S., Bidkhori, H.R., Doeppner, T.R., and Bahrami, A.R. (2021). Investigating the effects of IDO1, PTGS2, and TGF-β1 overexpression on immunomodulatory properties of hTERT-MSCs and their extracellular vesicles. Sci. Rep. *11*, 7825–7919. https://doi.org/10.1038/s41598-021-87153-7.
28. Kim, H.S., Lee, H.K., Kim, K., Ahn, G.B., Kim, M.S., Lee, T.Y., Son, D.J., Kim, Y., Hong, J.T., and Han, S.B. (2023). Mesenchymal stem cells enhance CCL8 expression by podocytes in lupus-prone MRL.Faslpr mice. Sci. Rep. *13*, 13074–13111. https://doi.org/10.1038/s41598-023-40346-8.
29. Yang, Y., Zhang, W., Wang, X., Yang, J., Cui, Y., Song, H., Li, W., Li, W., Wu, L., Du, Y., et al. (2023). A passage-dependent network for estimating the in vitro senescence of mesenchymal stromal/stem cells using microarray, bulk and single cell RNA sequencing. Front. Cell Dev. Biol. *11*, 998666. https://doi.org/10.3389/FCELL.2023.998666/FULL.
30. Sullivan, M., and Morgan, D.O. (2007). Finishing mitosis, one step at a time. Nat. Rev. Mol. Cell Biol. *8*, 894–903. https://doi.org/10.1038/nrm2276.
31. Beenken, A., and Mohammadi, M. (2009). The FGF family: biology, pathophysiology and therapy. Nat. Rev. Drug Discov. *8*, 235–253. https://doi.org/10.1038/NRD2792.
32. Raulf, N., Lucarelli, P., Thavaraj, S., Brown, S., Vicencio, J.M., Sauter, T., and Tavassoli, M. (2018). Annexin A1 regulates EGFR activity and alters EGFR-containing tumour-derived exosomes in head and neck cancers. Eur. J. Cancer *102*, 52–68. https://doi.org/10.1016/J.EJCA.2018.07.123.
33. Codrici, E., Albulescu, L., Popescu, I.D., Mihai, S., Enciu, A.M., Albulescu, R., Tanase, C., and Hinescu, M.E. (2018). Caveolin-1-Knockout Mouse as a Model of Inflammatory Diseases. J. Immunol. Res. *2018*, 2498576. https://doi.org/10.1155/2018/2498576.
34. Peng, B., Chen, Y., Wang, Y., Fu, Y., Zeng, X., Zhou, H., Abulaiti, Z., Wang, S., and Zhang, H. (2023). BTG2 acts as an inducer of muscle stem cell senescence. Biochem. Biophys. Res. Commun. *669*, 113–119. https://doi.org/10.1016/J.BBRC.2023.05.098.
35. Ermolaeva, M., Neri, F., Ori, A., and Rudolph, K.L. (2018). Cellular and epigenetic drivers of stem cell ageing. Nat. Rev. Mol. Cell Biol. *19*, 594–610. https://doi.org/10.1038/s41580-018-0020-3.
36. Li, Z., Xu, Z., Duan, C., Liu, W., Sun, J., and Han, B. (2018). Role of TCF/LEF Transcription Factors in Bone Development and Osteogenesis. Int. J. Med. Sci. *15*, 1415–1422. https://doi.org/10.7150/IJMS.26741.
37. Gregor, M.F., Misch, E.S., Yang, L., Hummasti, S., Inouye, K.E., Lee, A.H., Bierie, B., and Hotamisligil, G.S. (2013). The Role of Adipocyte XBP1 in Metabolic Regulation during Lactation. Cell Rep. *3*, 1430–1439. https://doi.org/10.1016/J.CELREP.2013.03.042.
38. Kadota, Y., Toriuchi, Y., Aki, Y., Mizuno, Y., Kawakami, T., Nakaya, T., Sato, M., and Suzuki, S. (2017). Metallothioneins regulate the adipogenic differentiation of 3T3-L1 cells via the insulin signaling pathway. PLoS One *12*, e0176070. https://doi.org/10.1371/JOURNAL.PONE.0176070.
39. Contreras, O., Córdova-Casanova, A., and Brandan, E. (2021). PDGF-PDGFR network differentially regulates the fate, migration, proliferation, and cell cycle progression of myogenic cells. Cell. Signal. *84*, 110036. https://doi.org/10.1016/J.CELLSIG.2021.110036.
40. Vaz, R., Martins, G.G., Thorsteinsdóttir, S., and Rodrigues, G. (2012). Fibronectin promotes migration, alignment and fusion in an in vitro myoblast cell model. Cell Tissue Res. *348*, 569–578. https://doi.org/10.1007/s00441-012-1364-1.
41. van der Fits, L., Mourits, S., Voerman, J.S.A., Kant, M., Boon, L., Laman, J.D., Cornelissen, F., Mus, A.M., Florencia, E., Prens, E.P., and Lubberts, E. (2009). Imiquimod-induced psoriasis-like skin inflammation in mice is mediated via the IL-23/IL-17 axis. J. Immunol. *182*, 5836–5845. https://doi.org/10.4049/jimmunol.0802999.
42. Pelham, R.J., Jr., and Wang, Y.l. (1997). Cell locomotion and focal adhesions are regulated by substrate flexibility. Proc. Natl. Acad. Sci. USA *94*, 13661–13665. https://doi.org/10.1073/pnas.94.25.13661.
43. Zhou, Y., Chen, H., Li, H., and Wu, Y. (2017). 3D culture increases pluripotent gene expression in mesenchymal stem cells through relaxation of cytoskeleton tension. J. Cell Mol. Med. *21*, 1073–1084. https://doi.org/10.1111/jcmm.12946.
44. Ichijo, R., Maki, K., Kabata, M., Murata, T., Nagasaka, A., Ishihara, S., Haga, H., Honda, T., Adachi, T., Yamamoto, T., and Toyoshima, F. (2022). Vasculature atrophy causes a stiffened microenvironment that augments epidermal stem cell differentiation in aged skin. Nat. Aging *2*, 592–600. https://doi.org/10.1038/s43587-022-00244-6.
45. Mascharak, S., desJardins-Park, H.E., Davitt, M.F., Griffin, M., Borrelli, M.R., Moore, A.L., Chen, K., Duoto, B., Chinta, M., Foster, D.S., et al. (2021). Preventing Engrailed-1 activation in fibroblasts yields wound regeneration without scarring. Science *372*, eaba2374. https://doi.org/10.1126/science.aba2374.
46. Li, Z., Liu, C., Xie, Z., Song, P., Zhao, R.C.H., Guo, L., Liu, Z., and Wu, Y. (2011). Epigenetic dysregulation in mesenchymal stem cell aging and spontaneous differentiation. PLoS One *6*, e20526. https://doi.org/10.1371/journal.pone.0020526.
47. Song, W.J., Li, Q., Ryu, M.O., Ahn, J.O., Ha Bhang, D., Chan Jung, Y., and Youn, H.Y. (2017). TSG-6 Secreted by Human Adipose Tissue-derived Mesenchymal Stem Cells Ameliorates DSS-induced colitis by Inducing M2 Macrophage Polarization in Mice. Sci. Rep. *7*, 5187–5214. https://doi.org/10.1038/s41598-017-04766-7.
48. Ko, J.H., Lee, H.J., Jeong, H.J., Kim, M.K., Wee, W.R., Yoon, S.O., Choi, H., Prockop, D.J., and Oh, J.Y. (2016). Mesenchymal stem/stromal cells precondition lung monocytes/macrophages to produce tolerance against allo- and autoimmunity in the eye. Proc. Natl. Acad. Sci. USA *113*, 158–163. https://doi.org/10.1073/PNAS.1522905113.
49. Molnarfi, N., Benkhoucha, M., Funakoshi, H., Nakamura, T., and Lalive, P.H. (2015). Hepatocyte growth factor: A regulator of inflammation and autoimmunity. Autoimmun. Rev. *14*, 293–303. https://doi.org/10.1016/j.autrev.2014.11.013.
50. Kida, Y.S., Kawamura, T., Wei, Z., Sogo, T., Jacinto, S., Shigeno, A., Kushige, H., Yoshihara, E., Liddle, C., Ecker, J.R., et al. (2015). ERRs mediate a metabolic switch required for somatic cell reprogramming to pluripotency. Cell Stem Cell *16*, 547–555. https://doi.org/10.1016/j.stem.2015.03.001.
51. Ylöstalo, J.H., Bartosh, T.J., Coble, K., and Prockop, D.J. (2012). Human mesenchymal stem/stromal cells cultured as spheroids are self-activated to produce prostaglandin E2 that directs stimulated macrophages into an anti-inflammatory phenotype. Stem Cell. *30*, 2283–2296. https://doi.org/10.1002/stem.1191.
52. Ding, Y., Gong, P., Jiang, J., Feng, C., Li, Y., Su, X., Bai, X., Xu, C., Liu, C., Yang, J., et al. (2022). Mesenchymal stem/stromal cells primed by inflammatory cytokines alleviate psoriasis-like inflammation via the TSG-6-neutrophil axis. Cell Death Dis. *13*, 996. https://doi.org/10.1038/s41419-022-05445-w.
53. Wagner, E.F., and Eferl, R. (2005). Fos/AP-1 proteins in bone and the immune system. Immunol. Rev. *208*, 126–140. https://doi.org/10.1111/j.0105-2896.2005.00332.x.
54. Hao, Y., Hao, S., Andersen-Nissen, E., Mauck, W.M., 3rd, Zheng, S., Butler, A., Lee, M.J., Wilk, A.J., Darby, C., Zager, M., et al. (2021). Integrated analysis of multimodal single-cell data. Cell *184*, 3573–3587.e29. https://doi.org/10.1016/j.cell.2021.04.048.
55. Saelens, W., Cannoodt, R., Todorov, H., and Saeys, Y. (2019). A comparison of single-cell trajectory inference methods. Nat. Biotechnol. *37*, 547–554. https://doi.org/10.1038/s41587-019-0071-9.
56. Li, Y., Dong, Y., Ran, Y., Zhang, Y., Wu, B., Xie, J., Cao, Y., Mo, M., Li, S., Deng, H., et al. (2021). Three-dimensional cultured mesenchymal stem cells enhance repair of ischemic stroke through inhibition of microglia. Stem Cell Res. Ther. *12*, 358. https://doi.org/10.1186/s13287-021-02416-4.
57. Love, M.I., Huber, W., and Anders, S. (2014). Moderated estimation of fold change and dispersion for RNA-seq data with DESeq2. Genome Biol. *15*, 550. https://doi.org/10.1186/s13059-014-0550-8.

STAR★METHODS

KEY RESOURCES TABLE

REAGENT or RESOURCE	SOURCE	IDENTIFIER
Antibodies		
FITC Mouse IgG1,K isotype Ctrl (1:50)	Biolegend	Cat#400108; clone MOPC-21; RRID: AB_326429
APC Mouse IgG1,K isotype Ctrl (1:50)	Biolegend	Cat#400122; clone MOPC-21; RRID: AB_326443
PE Mouse IgG1,K isotype Ctrl (1:50)	Biolegend	Cat#400112; clone MOPC-21; RRID: AB_2847829
APC anti-human CD73 (Ecto-5′-nucleotidase) (1:50)	Biolegend	Cat#344006; clone AD2; RRID: AB_1877157
APC anti-human CD90 (Thy1) (1:50)	Biolegend	Cat#328114; clone 5E10; RRID: AB_893431
APC anti-CD105 (Endoglin) (1:50)	Biolegend	Cat#800507; clone Sn6h; RRID: AB_2687060
FITC anti-human CD45 (1:50)	Biolegend	Cat#304006; clone HI30; RRID: AB_314394
FITC anti-human HLA-DR (1:50)	Biolegend	Cat#307603; clone L243; RRID: AB_314681
APC anti-human CD19 (1:50)	Biolegend	Cat#302211; clone HIB19; RRID: AB_314241
PE anti-human CD11b (1:50)	Biolegend	Cat#301305; clone ICRF44; RRID: AB_314157
FITC anti-human CD34 (1:50)	Biolegend	Cat#343603; clone 561; RRID: AB_1732030
BV421 Mouse Anti-Human CD3	BD	Cat#555332; clone UCHT1; RRID: AB_11152082
FITC Mouse Anti-Human CD8	BD	Cat#555634; clone HIT8a; RRID: AB_395996
PE Mouse Anti-Human IFN-γ	BD	Cat#559326; clone 4S.B3; RRID: AB_397223
PE anti-human IL-17A Antibody (1:50)	Biolegend	Cat#512306; clone BL168; RRID: AB_961394
Anti-Ki67 antibody (1:200)	Abcam	Cat#ab16667; clone SP6
Human TSG-6 Biotinylated Antibody	R&D	Cat#BAF2104; clone P98066
Bacterial and virus strains		
pLV-CBh-3FLAG-Luc2-tCMV-mNeonGreen-F2A-Puro	OBiO Technology	H7656
GPLVX-CMV-ZsGreen1	Genomeditech	GM100101
Biological samples		
Human perinatal placenta	Shenzhen People's Hospital	N/A
Chemicals, peptides, and recombinant proteins		
trypsin	Sigma	T4799-5G; CAS: 9002-07-7
polybrene	GenePharma	N/A; CAS: 28728-55-4
T5224	MedChemExpress	HY-122707; CAS: 530141-72-1
bovine serum albumin	Sigma	A1933-5G; CAS:9048-46-8
D-fluorescein	Sigma	46955-1G-F; CAS: 2321-07-5
phytohemagglutinin	Sigma	P1585-1MG; CAS: 16561-29-8
Ionomycin	Sigma	I3909-1ML; CAS: 56092-81-0
brefeldin A	Sigma	B5936-200UL; CAS: 20350-15-6
Triton X-100	Sangon	A600560-0500; CAS: 9005-64-5
Critical commercial assays		
Alizarin Red staining solution	Dakewe	4060611
Oil red staining solution	Dakewe	4060711
Alcian blue staining solution	Solarbio	G1560
lipid-forming differentiation medium	Dakewe	6114531
osteogenic differentiation medium	Dakewe	6114541
chondrogenic differentiation medium	Dakewe	6114551
RNAiso Plus reagent	Takara	9109

(*Continued on next page*)

Continued

REAGENT or RESOURCE	SOURCE	IDENTIFIER
Hifair II 1st Strand cDNA Synthesis SuperMix	Yeasen	11141ES60
Hieff UNICON® Universal Blue qPCR SYBR Green Master Mix	Yeasen	11184ES08
HGF ELISA Kit	4A Biotech	CHE0069
STC1 ELISA Kit	4A Biotech	CHE0317
H&E staining kit	Servicebio	G1005-500ML
imiquimod cream	Sichuan Mingxin	N/A
carboxyfluorescein diacetate succinimidyl ester	Thermo Fisher	C34554
Deposited data		
Raw and analyzed data	This paper	GEO:GSE268973
Code	This paper	Zenodo, https://doi.org/10.5281/zenodo.12742490
qPCR data	This paper	Shared upon request by the Lead Contact
Experimental models: Organisms/strains		
Mouse: C57BL/6	Weitonglihua Experimental Animal Technology	N/A
Oligonucleotides		
Primers for qPCR, see Table S1	This paper	N/A
Software and algorithms		
Seurat v4	Hao et al.[54]	https://github.com/satijalab/seurat
scRNAtoolvis	Zhang et al.	https://github.com/junjunlab/scRNAtoolVis
dynverse	Saelens et al.[55]	https://github.com/dynverse/dyno
Prism, Version 8.30	GraphPad	https://www.graphpad.com/scientific software/prism
R 4.1.3	R	https://www.r-project.org/

EXPERIMENTAL MODEL AND STUDY PARTICIPANT DETAILS

Mice

C57BL/6 female mice (7 weeks old) were purchased from Beijing Weitonglihua Experimental Animal Technology Co., Ltd., and housed in Tsinghua University Animal Center in specific pathogen-free conditions and all experimental animal protocols were approved by the Institutional Animal Care and Use Committee (IACUC) of Tsinghua University (Animal Protocol: 22-ZY1). The committees confirmed that all experiments conform to the relevant regulatory standards. The hairs of the dorsal skin (2 cm × 2 cm size) were removed using a depilatory cream. 24 h later, 80 mg 5% imiquimod (IMQ) cream (Sichuan Mingxin Pharmaceutical Co., Ltd.) was topically applied to the dorsal skin daily for 4 consecutive days.

METHOD DETAILS

MSC culture

MSCs was separated from the human virus pathogens-free perinatal placenta according to previously reported methods.[46,56] Ethics was approved by Ethics Committee of Shenzhen People's Hospital. Cells were cultured in monolayers in Dulbecco's modified Eagle's medium (DMEM; Corning) supplemented with 10% fetal bovine serum (FBS; ExCell Bio) at 37°C and 5% CO_2, and subcultured when reaching 85% confluence. MSCs in total passage 5–6 were subjected to 3D spheroid culture for 60 h in a culture spinner as previously described.[56] Briefly, single MSCs were suspended in a modified MSC growth medium and cultured in spinner flasks at 60 rpm. Spheroids in about 250 μm in diameter formed by 24 h and maintained for up to 60 h. To obtain single cells, the 3D cell spheres were collected and washed in PBS, digested with 0.05% trypsin containing 0.53 mM EDTA for 3–5 min at 37°C, and gently pipetted. For MSCs size comparing, 2D (Dil stained, red) and 3D (ZsGreen1 labeled, green) MSCs in passage 5–6 were digested into single cells, laid on a glass slide and imaged under a microscope in 5 random fields.

Transduction of MSCs (GFP/Luciferase)

Lentivirus pLV-CBh-3FLAG-Luc2-tCMV-mNeonGreen-F2A-Puro was purchased from OBiO Technology, Shanghai, China. GPLVX-CMV-ZsGreen1 was purchased from Genomeditech, Shanghai, China. Cells were grown overnight to 20% confluence and switched to

virus-containing medium with 2% FBS and 5 μg/mL polybrene. The culture was incubated for 6 h and switched to MSCs growth medium. Cells were examined under a fluorescence microscope for labeling efficiency up to 80% for experiments.

Flow cytometry

Single cells were resuspended in PBS containing 1% bovine serum albumin (BSA, Sigma) (1,000,000 cells/mL). 100 μL cell aliquots were incubated with antibodies against CD90, CD105, and CD73, CD34, CD11b, CD19, CD45, and HLA-DR (Biolegend) on ice for 30 min. Samples were analyzed on a BD C6 Plus flow cytometer, and 10,000 events were collected.

Trilineage differentiation

MSCs cultured in monolayers (2D) to passage 5–6 were subjected to 3D spheroid culture. Single MSCs before and after 3D culture were seeded into 12-well plates with 150,000 cells per well in 1.5 mL DMEM supplemented with 10% FBS and incubated for 24 h. For adipogenesis, cells were then cultured in lipid-forming differentiation medium (Dakewe), which was changed every 3 days until 21 days. Subsequently lipid was stained with oil red. For osteogenesis, cells were then cultured in osteogenic differentiation medium (Dakewe), which was changed every 3 days until 21 days. Calcium deposits were subsequently stained with Alizarin Red. For chondrogenesis, 1 million 2D MSCs were centrifuged to form a pellet, which was incubated in chondrogenic differentiation medium (Dakewe). The medium was changed every 3 days until 21 days. Subsequently the pellet was sectioned and stained with Alcian blue(Solarbio).

Bioluminescence imaging

One million 2D or 3D cultured human placental MSCs expressing luciferase were injected through the tail vein of Balb/C mice. Mice were intraperitoneally injected with 150 mg/kg D-fluorescein and anesthetized with isoflurane. Bioluminescence signals were detected 24 h after cell transplantation using Bruker spectrum imaging system, and the total number of photons was quantified as P/S/cm2/sr.

Bulk RNA sequencing and quantitative real-time PCR (qPCR)

MSCs were cultured in 2D monolayers to passage 5–6. Cells in about 85% confluence were lysed in plates in RNAiso Plus reagent (Takara) and stored at −80°C. MSCs in the same passage of the same donor were cultured in 3D spheroids for 60 h, and the spheres were collected and lysed in RNAiso Plus reagent. The samples were sent to Wuhan BGI Gene Technology Service Company (Wuhan, China) in dry ice for RNA extraction, library construction and sequencing. The results were analyzed with DESeq2[57] in R studio. For qPCR analysis, RNA was quantified using Nanodrop (Thermo Scientific) and cDNA was synthesized from 2 μg of total RNA with Hifair II 1st Strand cDNA Synthesis SuperMix for qPCR (Yeasen). Subsequently, qPCR was performed on instrument CFX96 (Bio-Rad) using Hieff UNICON Universal Blue qPCR SYBR Green Master Mix (Yeasen) in 96 well-plate(NEST). The relative mRNA expression of target genes was analyzed according to the $2^{-\Delta\Delta CT}$ method and normalized to the level of reference gene *GAPDH*. Primers were synthesized by Ruibotech(Guangzhou, China) and all primer sequences were shown in Table S1.

Single-cell RNA sequencing (scRNA-seq)

MSCs were cultured in 2D monolayers to passage 5. Cells in about 85% confluence were trypsinized into single cells. MSCs in the same passage of the same donor were cultured in 3D spheroids for 60 h, and the cell spheres were collected and trypsinized into single cells. The single cells were sequenced by Oebiotech (Shanghai, China) on a 10× Genomic platform. scRNA data analysis code is supplemented. In brief, the two datasets were analyzed and integrated with Seurat v4.[54] Variable markers of each cluster are analyzed by scRNAtoolvis package (https://github.com/junjunlab/scRNAtoolVis). Gene ontology enrichment was carried out with enrichR function and GO_2023 as reference. Trajectory analysis was performed using dynverse (https://github.com/dynverse/dynbenchmark)[55] and slingshot method.

PBMC stimulation and CFSE assay

For testing lymphocyte proliferation, equal numbers of 2D or 3D MSCs were co-cultured with phytohemagglutinin (PHA, purchased from Sigma)-activated human peripheral blood mononuclear cells (PBMCs) which were labeled by carboxyfluorescein diacetate succinimidyl ester (CFSE, Thermo Fisher Scientific) for 96 h, and the effects of MSCs on the proliferation of total lymphocytes were evaluated according to the changes in CFSE fluorescence intensity determined by flow cytometry.

For testing Th17 differentiation, 1 × 10^6 fresh PBMCs were co-cultured with 3D MSCs or 2D MSCs in 5:1 ratio, and incubated in a CO2 incubator for 20 h. Then add 25 ng/mL PMA, 1 μg/mL Ionomycin (Sigma) and 10 μg/mL brefeldin A (BFA, Sigma). After 4 h of culture, the PBMCs in each well were collected and stained at room temperature for 30 min with CD8 and CD3 antibodies (BD). Then, IFN-γ, IL-4 and IL-17A antibodies (BD) were added respectively, and incubated for 30 min in dark. The cells were washed twice with PBS, and analyzed using a BD C6 Plus flow cytometer. The $CD3^+CD8^-$IL-$17A^+$cells were identified as Th17 subpopulation. Statistical analysis were carried out by normalizing the Th17 proportion in the treated groups against the average value of Th17 proportion in PBMC.

Cytokine quantification by ELISA

2D MSCs in passage 5–6 were cultured in monolayers to 85% confluence. MSCs in the same passage were cultured in 3D spheroids for 60 h. 2D and 3D MSCs were harvested and trypsinized into single cells. Equal numbers of 2D MSCs and 3D MSCs were seeded into tissue culture

plates and maintained in MSCs growth medium for 16 h to reach about 70% confluence. Then the medium was changed to serum-free basal medium and incubated for 24 h. The conditioned media were collected and centrifuged at 2095 g for 30 min at 4°C. The supernatants were collected and subjected to ELISA analysis for the levels of TSG6 (R&D), HGF (4A Biotech) and STC1 (4A Biotech) using corresponding kits following the manufacturers' instructions.

Histology

Paraffin sections of the skin tissue in 5 μm thickness were subjected to hematoxylin and eosin (H&E) staining using a kit (Servicebio) according to the manufacture' instructions. For immunofluorescence staining, tissue cryosections were wash with PBS and blocked in a buffer containing 0.1% Triton X-100 (Sangon) and 1% BSA. Samples were then incubated with a primary antibody against Ki-67 (Abcam) at 4°C overnight, washed with PBS and detected with a fluorescence-conjugated secondary antibody. After nuclear staining with DAPI, samples were mounted and visualized under a confocal microscope (CQ1, YOKOGAWA).

MSCS ADMINISTRATION TO PSORIASIS MOUSE MODEL

1 × 10^6 2D MSCs, 1 × 10^6 3D MSCs, or 5 × 10^6 3D MSCs in 200 μL PBS were intravenously injected through the tail vain 24 h prior to IMQ treatment. In the control group, equal amount of PBS was injected. In some mice, 5 × 10^6 3D MSCs expressing GFP were injected to trace MSCs distribution. Mice were observed daily for changes (color, scales and wrinkles) in the skin and photographed. On the 2nd and 4th days of IMQ treatment, full thickness skin tissues of the treated area were harvested for histological analysis. The severity of the skin psoriasis-like lesion was assessed and scored according to the Psoriasis Area and Severity Index (PASI) based on intensity of redness, thickness, and scaling of the treated skin area, from 0 to 4: none 0; slight 1; moderate 2; marked 3; very marked 4.

QUANTIFICATION AND STATISTICAL ANALYSIS

All values were expressed as means ± SD. Comparison between two groups was performed with two-tailed Student's t test. Comparisons among more than two groups were performed using one-way analysis of variance (ANOVA). Differences were considered statistically significant when $p < 0.05$. Statistical analysis were conducted by Prism 8.30 (GraphPad Software, San Diego, CA, USA).